Regenerative Therapy 25 (2024) 331–343

Contents lists available at ScienceDirect

Regenerative Therapy

journal homepage: http://www.elsevier.com/locate/reth

Original Article

Effect of acidosis on adipose-derived stem cell impairment and gene expression

Kun Huang [a, 1], Qinqin Wang [a, 1], Huilong Qu [a, 1], Xinyu Hu [b], Wenhao Niu [a], Anna Hultgårdh-Nilsson [c], Jan Nilsson [d, ***], Chun Liang [a, **], Yihong Chen [a, c, *]

[a] Department of Cardiology, Second Affiliated Hospital of Naval Medical University, Shanghai Cardiovascular Institute of Integrative Medicine, 200003 Shanghai, China
[b] Institute for Molecules and Materials, Radboud University, Nijmegen 6525 AJ, Netherlands
[c] Department of Experimental Medical Science, Lund University, 22184 Lund, Sweden
[d] Department of Clinical Sciences Malmö, Lund University, 20502 Malmö, Sweden

ARTICLE INFO

Article history:
Received 4 December 2023
Received in revised form
10 January 2024
Accepted 25 January 2024

Keywords:
Adipose-derived stem cells
Ischemia
Acidosis
pH regulation
Angiogenesis

ABSTRACT

Based on disappointing results of stem cell-based application in clinical trials for patients with critical limb ischemia, we hypothesized that the acidic environment might be the key factor limiting cell survival and function. In the present study, we used microdialysis to determine presence of acidosis and metabolic imbalance in critical ischemia. Moreover, we explored the effect of extracellular acidosis on adipose-derived stem cells (ADSCs) at molecular and transcriptional level. Our data demonstrate that low pH negatively regulates cell proliferation and survival, also, it results in cell cycle arrest, mitochondrial dynamics disorder, DNA damage as well as the impairment of proangiogenic function in a pH-dependent manner. Further transcriptome profiling identified the pivotal signaling pathways and hub genes in response to acidosis. Collectively, these findings provide strong evidences for a critical role of acidosis in ADSCs impairment with ischemic condition and suggest treatments focus on tissue pH balance and acidosis-mediated hub genes may have therapeutic potential in stem cell-based application.

1. Introduction

In peripheral arterial disease (PAD), flow restriction is mainly due to atherosclerosis and thrombus leading to lower limb ischemia. Critical limb ischemia (CLI) is regarded as the most severe stage of PAD, with a mortality rate of around 20 % within 6 months from diagnosis in patients for whom revascularization is possible [1,2], while in 20 %–50 % CLI patients for whom revascularization is impossible [3,4] the mortality rate ups to 40 % within just one year [3,5]. Thus, there is an urgent need to develop novel therapies to

Abbreviations: PAD, peripheral arterial disease; CLI, critical limb ischemia; LDPI, laser doppler perfusion imaging; ADSC, adipose-derived stem cells; FUCCI, fluorescence ubiquitination-based cell cycle indicator; Tomm20, translocase of outer mitochondrial membrane 20; PI, propidium iodide; HUVECs, human umbilical vein endothelial cells; qRT-PCR, quantitative real-time PCR; DEGs, differentially expressed genes; GO, gene ontology; KEGG, Kyoto encyclopedia of genes and genomes; PPI, protein–protein interaction; ECM, extracellular matrix; STRING, search tool for the retrieval of interacting genes; MCC, maximal clique centrality; VEGF-A, vascular endothelial growth factor A; CDKN1A, cyclin dependent kinase inhibitor 1A; E2F7, E2F transcription factor 7; CRK, CRK proto-oncogene, adaptor protein; MMP2, matrix metallopeptidase 2; ABL1, ABL proto-oncogene 1, non-receptor tyrosine kinase; IL-6, interleukin 6; CDC42, cell division cycle 42; KRAS, KRAS proto-oncogene, GTPase; SHC1, SHC adaptor protein 1; PIK3R1, phosphoinositide-3-kinase regulatory subunit 1; TP53, tumor protein p53.

* Corresponding author. Department of Cardiology, Second Affiliated Hospital of Naval Medical University, Shanghai Cardiovascular Institute of Integrative Medicine, No. 415, Fengyang Road, 200003 Shanghai, China.
** Corresponding author. Department of Cardiology, Second Affiliated Hospital of Naval Medical University, Shanghai Cardiovascular Institute of Integrative Medicine, No. 415, Fengyang Road, 200003 Shanghai, China.
*** Corresponding author. Department of Clinical Sciences Malmö, Lund University, JanWaldenströms gata35, 20502 Malmö, Sweden.
E-mail addresses: jan.nilsson@med.lu.se (J. Nilsson), chunliangliang1985@163.com (C. Liang), yihong.chen@med.lu.se (Y. Chen).
Peer review under responsibility of the Japanese Society for Regenerative Medicine.
[1] Contributed equally to this work.

https://doi.org/10.1016/j.reth.2024.01.010

improve the outcome in non-revascularizable patients. Stem cell-based therapy is a promising option in this regard. A growing number of pro-clinical studies suggest that stem cell-based therapy may offer a safe and effective approach to promote angiogenesis and blood flow recovery [6–11], acting not only on paracrine functions [12–14], but also on differentiation and vessel formation [14,15]. However, results from several clinical trials of stem cell transplanting have failed to meet expectations and did not result in reduced amputation rates [16–18].

A key factor in these studies is the poor stem cell survival in the ischemic microenvironment [19–22]. Specifically, the tissue ischemia of CLI patients suffering from diabetes is particularly problematic, due to the chronic metabolic dysfunction [21]. Tissue acidosis, a common characteristic feature of ischemia and inflammation can affect the function and survival of transplanted cells [22]. Previous studies showed that the mean muscle surface pH in patients with ischemic gangrene is decreased to 6.85, at the same time, the alteration of tissue pH precedes changes in arterial flow [23]. Likewise, another evidences indicated that the ischemic tissue pH varies substantially between CLI patients which potentially may be importance for local energy metabolism, cell viability, senescence and apoptosis [24,25].

In this study, we analyzed the effect of critical hindlimb ischemia on tissue metabolism by microdialysis and confirmed the presence of acidosis in ischemic areas. Human adipose-derived stem cells (ADSCs) were cultured with conditions ranging from a pH of 7.4 to 6.5, to explore the effect of extracellular acidosis at molecular and transcriptional level. This study expands our knowledge of stem cell physiology and angiogenic function in ADSCs with acidic environments and suggests possible options for future stem cell-based therapy.

2. Methods

2.1. Induction of hindlimb ischemia and laser Doppler perfusion imaging (LDPI)

BALB/c nude male mice at an age of 10 weeks were purchased from the Institute of Laboratory Animal Science CAMS & PUMC (Beijing, China) and kept in the animal center of Naval Medical University in a 12-h light/dark cycle, with sterilized food and water ad libitum during the experimental period. All procedures on animals were approved by the Ethics Review of Animal Use Application of Naval Medical University and conducted in conformity with the National Institutes of Health Guidelines for the Care and Use of Laboratory Animals. The generation of mouse model with hindlimb ischemia was performed as previous report [26]. In this case, the left hindlimbs of nude mice were treated as ischemic ones, and the right femoral arteries were exposed without damage as the non-ischemic controls. To evaluate blood flow and confirm the success of the ischemia models, LDPI (Perimed Instruments AB, Sweden) was conducted on mice immediately before and after surgery. Briefly, the anesthetized mice with oxygen-carried isoflurane were placed on a homeothermic heating pad and blood flow perfusion was quantified via scanning an equal area of both hindlimbs by LDPI: blood flow ratio = ischemic limb perfusion (left hindlimb)/ non-ischemic limb perfusion (right hindlimb) × 100 %.

2.2. Microdialysis

The theory and protocol of microdialysis have been reported clearly before [27]. Due to the existence of a concentration gradient, extracellular metabolites were diffused via a double-lumen probe with an integrated semipermeable membrane. The concentration of target molecules was measured in the microdialysis solution equilibrated with the surrounding tissue fluid, to gauge the level of metabolism in the tissues. In our study, a double-lumen microdialysis probe with a membrane (0.5 mm diameter, 10 mm length and 20.00 kDa molecular weight cut off) (CMA 20, CMA Microdialysis, Sweden), which connected to a precision infusion pump (CMA 102, CMA Microdialysis, Sweden), was used to collect the microdialysis solution by exchanging with physiological saline solution at a flow rate 2 μl/min. To minimize the impact from probe insertion damage, microdialysis solution was equilibrated for 30 min [28] after probe imbedding hind limb muscle, then collected to be analyzed by CMA 600 Microdialysis Analyser (CMA Microdialysis, Sweden). In this case, we detected the concentrations of lactate and glucose in microdialysis liquid from the hind limb muscles after surgery. The recovery rates [29] were also determined with a calibration solution (2.50 mmoL/l lactate and 5.55 mmoL/l glucose) ordered from CMA Microdialysis for calculating the practical concentration of substances *in vivo*.

2.3. Cell culture and acidic treatments

The ADSCs were obtained from QuiCell (Shanghai, China). Cells were maintained in DMEM/F12 (Gibco, USA) supplemented with 10 % fetal bovine serum (FBS, Gibco, USA) or mesenchymal stem cell medium (MSC, ScienCell, USA) contained 5 % FBS and 1 % mesenchymal stem cell growth supplement (MSCGS, ScienCell, USA). Penicillin and streptomycin (1 %, Gibco, USA) were always appended in the culture medium. ADSCs at passage 3–6 were chosen for further experiments in this study. The pH of the complete culture medium was measured as 7.4 using a pH meter (Wiggens, Germany). For the stability of pH treatment, additional HEPES buffer (Gibco, USA) was added into the culture medium for a concentration of 25 mM. Then the medium was adjusted with pre-calculated volumes of HCL (Sigma–Aldrich) to achieve the indicated pH (pH = 7.2, 7.0 and 6.5) as acidic treatment.

2.4. Fluorescence ubiquitination-based cell cycle indicator (FUCCI) system and live cell time-lapse images

The plasmid of pBOB-EF1-FastFUCCI-Puro (RRID: Addgene 86849) fusing the fluorescent probes of mKO2-hCDT1 and mAG-hGEM was subjected to track the stage of cell cycle. After plasmids transfection and lentiviral transduction, stable FUCCI-expression ADSCs were obtained via introduction of FUCCI system into ADSCs, which indicated cells in G1 phase, the G1/S transition phase, and S and/or G2-M phases as red, yellow and green as previous reports [30,31]. The time-lapse images of live cells with low pH stimulation for 48 h were recorded using an inverted widefield fluorescence microscope (Zeiss, Axio Observer, Germany) equipped with an incubation chamber.

2.5. Immunofluorescence staining

Cells on coverslips were fixed with 4 % paraformaldehyde for 12 min and permeabilized with 0.5 % Triton X-100 after washing with DPBS. Then samples were blocked with 3 % bovine serum albumin (Sigma–Aldrich, USA) for 60 min at room temperature and stained with primary antibodies at 4 °C overnight. On the second day, samples were incubated with the Cy3 -conjugated (167416, 1:1000, Jackson, USA) or ALEXA 480 conjugated (166,827, 1:1000, Jackson, USA) secondary antibodies for 60 min at room temperature. Nuclei were labeled with 4′,6-diamidino-2-phenylindole dihydrochloride (DAPI, 1 μg/μl, Sigma–Aldrich, USA). The primary antibodies were listed: Ki67 (ab16667, 1:100, Abcam, UK), Lamin B1 (ab16048, 1:500, Abcam, UK), Tomm 20 (PA5-52843, 1:100, Thermos Fisher, USA). The images were recorded using a Nikon A1R

confocal microscope (Nikon, USA) and analyzed with ImageJ software. Data were obtained from 3 independent replicates of each group. For $Ki67^+$ counting, we used 8 random fields from 4 different wells per group for each repeat, at least 738 cells were analyzed each condition. For measurement of mitochondrial length, results were quantified from at least 30 cells every group.

2.6. Cell cycle and cell apoptosis

Cell samples with specific acidic treatment for 48 h were dissociated from 6-well plates and washed twice with pre-cold DPBS. For cell cycle analysis, 1 ml DPBS was used to resuspend cells after centrifugation. Cells were fixed by dropping into 4 ml pre-cold 70 % ethanol in DPBS and kept at −20 °C for at least 24 h. After that, the samples were centrifuged and washed again, followed by staining with 20 μg/ml propidium iodide (PI, Sigma–Aldrich, USA) in DPBS containing 10 μg/ml RNase for 30 min in the dark. The APC Annexin V kit (BD, USA) and PI were performed to determine cell apoptosis. According to the manufacturer's instructions, binding buffer was used to resuspend ADSCs and 100 μl of the solution containing 10^5 cells was transferred to a new tube. After staining with APC Annexin V and PI for 15 min in the dark, an additional 400 μl of binding buffer was added to each tube. All samples were analyzed by flow cytometry (BD, USA). Data were calculated by FlowJo and ModFit LT software.

2.7. Cell viability and caspase-Glo 3/7 assay

The CellTiter-Glo Luminescent Cell Viability Assay and Caspase-Glo 3/7 Assay (Promega, USA) were performed to evaluate ADSCs viability and apoptosis. Cells were seeded at 3×10^3/well on 96-well plates. For cell viability assessment, ADSCs were conducted with acidic treatments for 0, 24 and 48 h. For cell apoptosis assay, the acidic conditions on cells were maintained for 48 h. Subsequent steps were performed following the manufacturer's instructions. Data were read by the GloMax-Multi Detection System (Promega, USA).

2.8. Enzyme-linked immunosorbent assay (ELISA)

Culture medium from ADSCs with acidic exposures for 48 h was collected to measure secreted vascular endothelial growth factor A (VEGF-A) protein. The level of released protein was detected with Human VEGF-A Elisa Kit (RayBio, USA) according to the manufacturer's protocols. Data was read at 450 nm using Synergy h1 microplate reader (BioTek, USA).

2.9. Tube formation

Human umbilical vein endothelial cells (HUVECs) on 6-well plates were starved with medium 200 (Gibco, USA) containing 0.5 % low serum growth supplement (LSGS, Gibco, USA) for 24 h. TrypLE Express (Gibco, USA) was used to dissociate adherent cells. After centrifuge, endothelia cells were resuspended in collected culture medium from ADSCs stimulated by specific pH condition for 48 h. Next, cells with different treatment were seeded at a density of 1.0×10^4/well in μ-Slide Angiogenesis (Ibidi, USA) pro-coated with Geltrex reduced growth factor basement membrane matrix (Gibco, USA). After 12 h of incubation, randomized images were captured using an inverted microscope (Nikon, Eclipse TE2000-U, Japan) and the quantifiable measurement was performed by ImageJ software with Angiogenesis Analyzer plug-in (pixel/unit).

2.10. Quantitative real-time PCR (qRT-PCR) and RNA-sequencing analysis

ADSCs on 6-well plates treated with different pH condition for 24 h or 48 h were lysed with Trizol reagent (Invitrogen, CA, USA) to extract the total RNA. Then synthesis of cDNA and qRT-PCR reaction were carried out with miScript II RT kit and miScript SYBR Green PCR kit (Qiagen, Valencia, CA). All primers were purchased from qSTAR qPCR primer pairs (OriGene, USA). The mRNA expression of GAPDH from samples was used as endogenous control for normalization. The sequences of primers were listed in Table 1. For RNA-sequencing analysis, all the processes including mRNA enrichment, reverse transcription after RNA fragment, end repair, A tailing adding, adaptor ligation, PCR amplification, denaturing and cyclization, and sequencing on BGISEQ-500 platform were performed at BGI. Tech (Shenzhen, China). The filtered clean reads were mapped to reference using Bowtie2 [32], then the levels of gene and isoform expression were calculated by RSEM [33]. Finally, the differentially expressed genes (DEGs) were detected basing on FPKM values. In this study, we used Morpheus (https://software.broadinstitute.org/morpheus/) to show DEGs between control and acidic groups. DAVID (https://david.ncifcrf.gov/) was carried out to analyze gene ontology (GO) and kyoto encyclopedia of genes and genomes (KEGG) pathway enrichment. ToppCluster online tool (https://toppcluster.cchmc.org/) was used to analyze the functional enrichment and reveal the interaction network among DEGs. Pathways and gene ontologies containing molecular functions, biological process and cellular component were selected to identify the enrichment of gene modules. The top modules with the greatest gene enrichment score 10 were performed to generate the protein–protein interaction (PPI) networks and Cytoscape (v3.9.1) software was applied to visualize the cluster network maps.

2.11. Statistical analyses

GraphPad Prism 9.0 software was performed to analyze experimental data. Data was presented as means ± standard deviation (SD) in Fig. 1 and presented as means ± standard error of mean (SEM) in other figures. Student's unpaired *t* test was used to assess the differences between two groups, one-way ANOVA with Dunnett's multiple comparisons test was carried out for a single control

Table 1
Primers used in the present study for qRT-PCR.

Accession number	Gene	Sequence (5′–3′)
NM_001025366	VEGF-A-F	TTGCCTTGCTGCTCTACCTCCA
	VEGF-A-R	GATGGCAGTAGCTGCGCTGATA
NM_001791	CDC42-F	TGACAGATTACGACCGCTGAGTT
	CDC42-R	GGAGTCTTTGGACAGTGGTGAG
NM_033360	KRAS-F	CAGTAGACACAAAACAGGCTCAG
	KRAS-R	TGTCGGATCTCCCTCACCAATG
NM_183001	SHC1-F	ACAGCCGAGTATGTCGCCTATG
	SHC1-R	CAATGGTGCTGATGACATCCTGG
NM_181523	PIK3R1-F	CGCCTCTTCTTATCAAGCTCGTG
	PIK3R1-R	GAAGCTGTCGTAATTCTGCCAGG
NM_000546	TP53-F	CCTCAGCATCTTATCCGAGTGG
	TP53-R	TGGATGGTGGTACAGTCAGAGC
NM_007313	ABL1-F	CCAGGTGTATGAGCTGCTAGAG
	ABL1-R	GTCAGAGGGATTCCACTGCCAA
NM_016823	CRK-F	CCAATGCCTACGACAAGACAGC
	CRK-R	TGGGAAGTGACCTCGTTTGCCA
NM_000600	IL-6-F	AGACAGCCACTCACCTCTTCAG
	IL-6-R	TTCTGCCAGTGCCTCTTTGCTG
NM_004530	MMP-2-F	AGCGAGTGGATGCCGCCTTTAA
	MMP-2-R	CATTCCAGGCATCTGCGATGAG
NM_002046	GAPDH-F	GTCTCCTCTGACTTCAACAGCG
	GAPDH-R	ACCACCCTGTTGCTGTAGCCAA

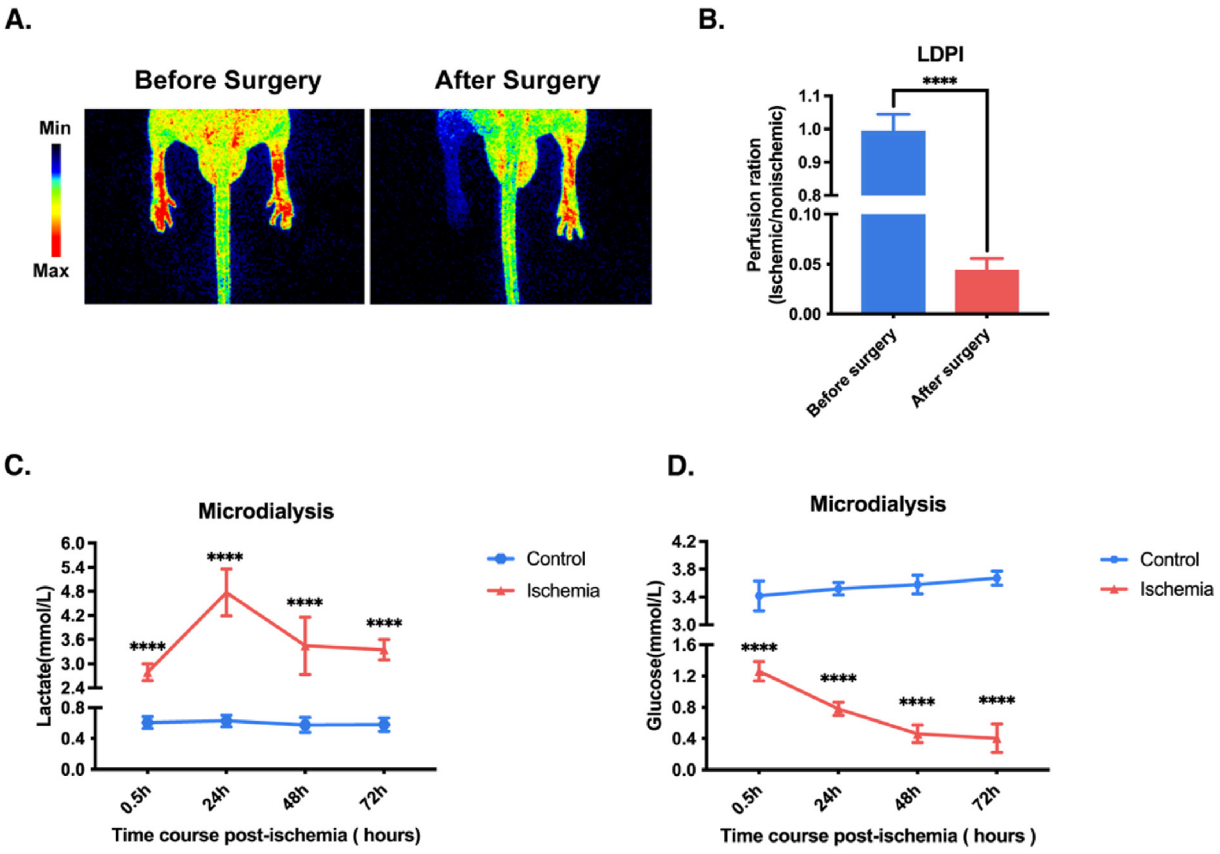

Fig. 1. Microdialysis revealed the raised lactate and reduced glucose level in hindlimb muscle after ischemia. **(A)** Representative images showed the blood flow in hindlimbs before and after femoral artery ligation. **(B)** The blood perfusion was evaluated by scanning an equal area of both hindlimbs using laser doppler perfusion imaging (LDPI) and quantified as the ratio of ischemic (right) to non-ischemic (left) side of hindlimb. **(C–D)** Microdialysis detecting displayed the concentration of lactate **(C)** and glucose **(D)** in hindlimb muscle at 0.5 h, 24 h, 48 h and 72 h of post-ischemia. The level of lactate and glucose in non-ischemic hind limbs was used as respective control. Data are presented as means ± standard deviation (SD), n = 5–6 per group. Student's unpaired *t* test for B, two-way ANOVA followed with Sidak's multiple comparisons test for C and D.

and each of a number of treated groups. For Microdialysis experiment, two-way ANOVA followed with Sidak's multiple comparisons test was used. Results were considered significant at $P < 0.05$.

3. Results

3.1. Microdialysis revealed the raised lactate and reduced glucose level in hindlimb muscle after ischemia

To research the alteration of metabolic microenvironment in response to ischemia in hindlimbs, a mouse model with hindlimb ischemia and microdialysis technology were performed. The ligation of femoral artery led to a decrease on blood flow by around 95 %, which confirmed by noninvasive LDPI evaluation (Fig. 1A, B). The concentration of lactate and glucose in non-ischemic hind limbs was detected as control level of muscular lactate and glucose *in vivo*, respectively (Fig. 1C, D). An increased lactate level was observed at 30 min after induction of ischemia. During 0.5–72 h of post-ischemia, the content of extracellular lactate in the hindlimb was consistently higher than it in control side. It is interesting to note that the lactate level reaches the peak value of 4.77 ± 0.58 mmol/L at 24 h after femoral artery occlusion, which is more than sevenfold higher than control value at the same time-point. In sharp contrast, the muscular glucose level was decreased at the first 0.5 h following ischemia and continued to reduce during 72 h of ischemia (Fig. 1. C) . At the end-point of detection, the glucose level in ischemic muscle tissue lowered at 0.40 ± 0.18 mmol/L, whereas that in control tissue maintained at 3.67 ± 0.10 mmol/L. All data of microdialysis was calibrated with recovery rates.

3.2. Extracellular acidosis affected cell proliferation, cell apoptosis and cell cycle in ADSCs with a pH-dependent manner

With the acidification of culture medium, a decreased ADSCs proliferation was identified by Ki67 staining in a pH-dependent way (Fig. 2A). Only 30 % of ADSCs were still in cell cycle ($Ki67^{+}$) after incubation with medium at pH 6.5 for 48 h, however, the percentage in the control group was 85 % (Fig. 2B). Consistent with the Ki67 index, a reduced cell viability was also observed at pH 7.0 and 6.5 conditions (Fig. 2C). Next, we investigated the effect of extracellular acidosis on cell apoptosis using flow cytometry and activated caspase-3/-7 detection. The moderate acidic environments did not affect cell apoptosis, however, the percentage of Annexin V + cells was significantly enhanced when the pH was lowered to 6.5 and this was associated with a ~10 % increase in frequency apoptotic cells (Fig. 2D). In line with the data from flow cytometry analysis, acidosis-mediated apoptosis at the lowest pH group was also confirmed by the elevated level of active caspase-3/-7 (Fig. 2E). There were some evidences to indicate that acidosis induces quiescent phenotype in cancer cells and dental pulp stem cells [34]. To confirm this in ADSCs, a FUCCI system was established to monitor the progression of cell cycle in live cells with low pH stimulations. The FUCCI system depends on the combination of 2

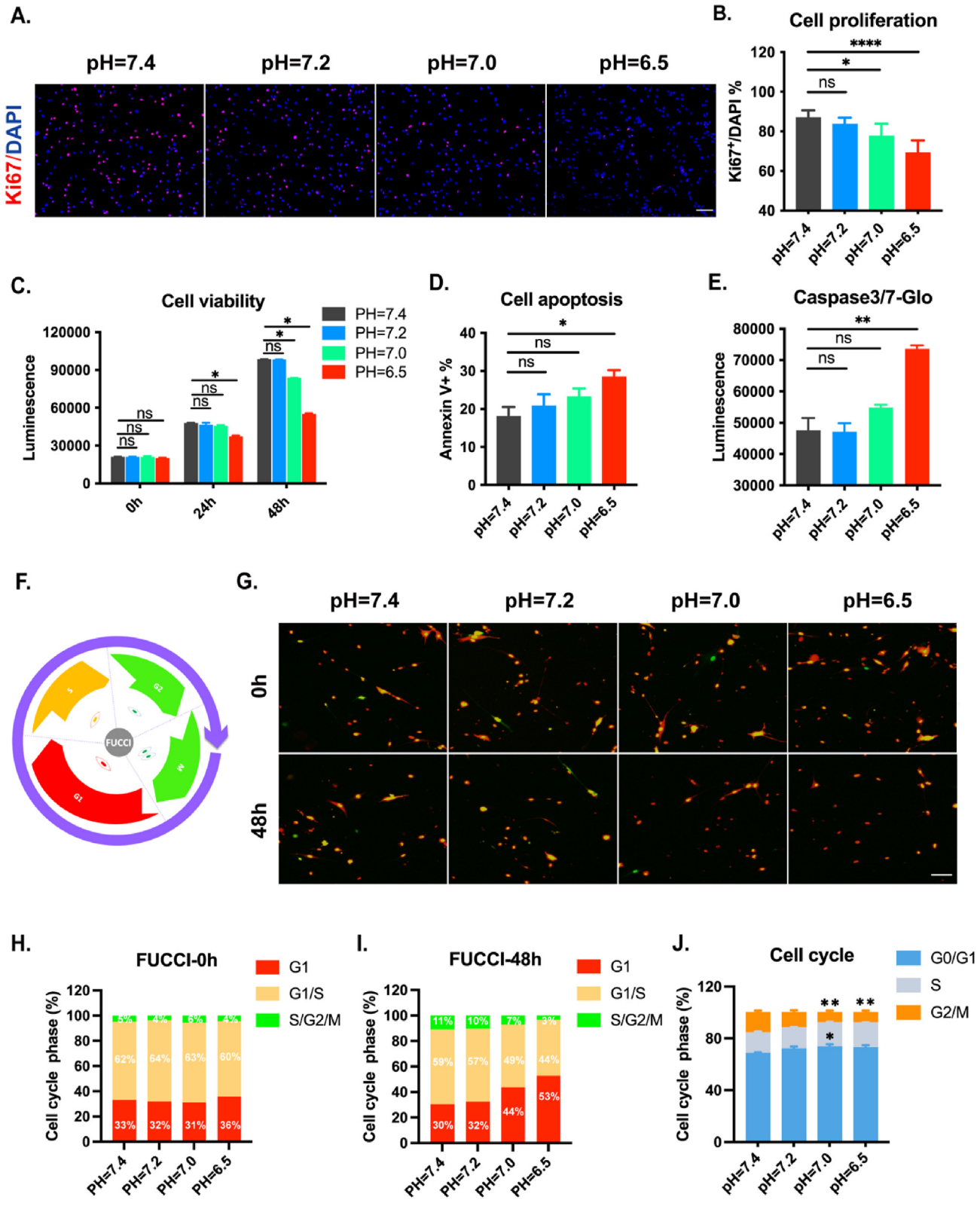

Fig. 2. Extracellular acidosis suppressed cell proliferation and viability, induced cell apoptosis and cell cycle arrest in ADSCs using a pH-dependent manner. **(A)** Representative images of Ki67 and DAPI staining in ADSCs incubated with culture medium at indicated pH (scale bar = 100 μm). **(B)** The quantification of Ki67^{+} index was performed to evaluate cell proliferation**. (C)** The ATP production of active cells with different pH treatments for 0 h, 24 h and 48 h were assessed by luminescent signals. **(D–E)** Cell apoptosis induced by acid exposure for 48 h was determined by APC Annexin V plus PI staining and luminescent signals of activate of caspase-3 and caspase-7. **(F)** Cell cycle-dependent changes of fluorescence in ADSCs applied with cell cycle reporter FUCCI system. **(G)** Representative pictures of cell cycle progression in ADSCs with acid exposure for 0 h and 48 h. Cells in G1, G1/S, and S/G2/M displayed as red, yellow and green (scale bar = 100 μm). **(H-I)** The distribution of cell cycle phases in ADSCs with different pH treatments based on Fucci system. **(J)** Flow cytometry analysis of ADSCs cultured with the specific pH condition for 48 h using PI staining. Data are presented as means ± SEM, **P < 0.01, ***P < 0.001, and ****P < 0.0001 by one-way ANOVA and Dunnett's post-hoc test.

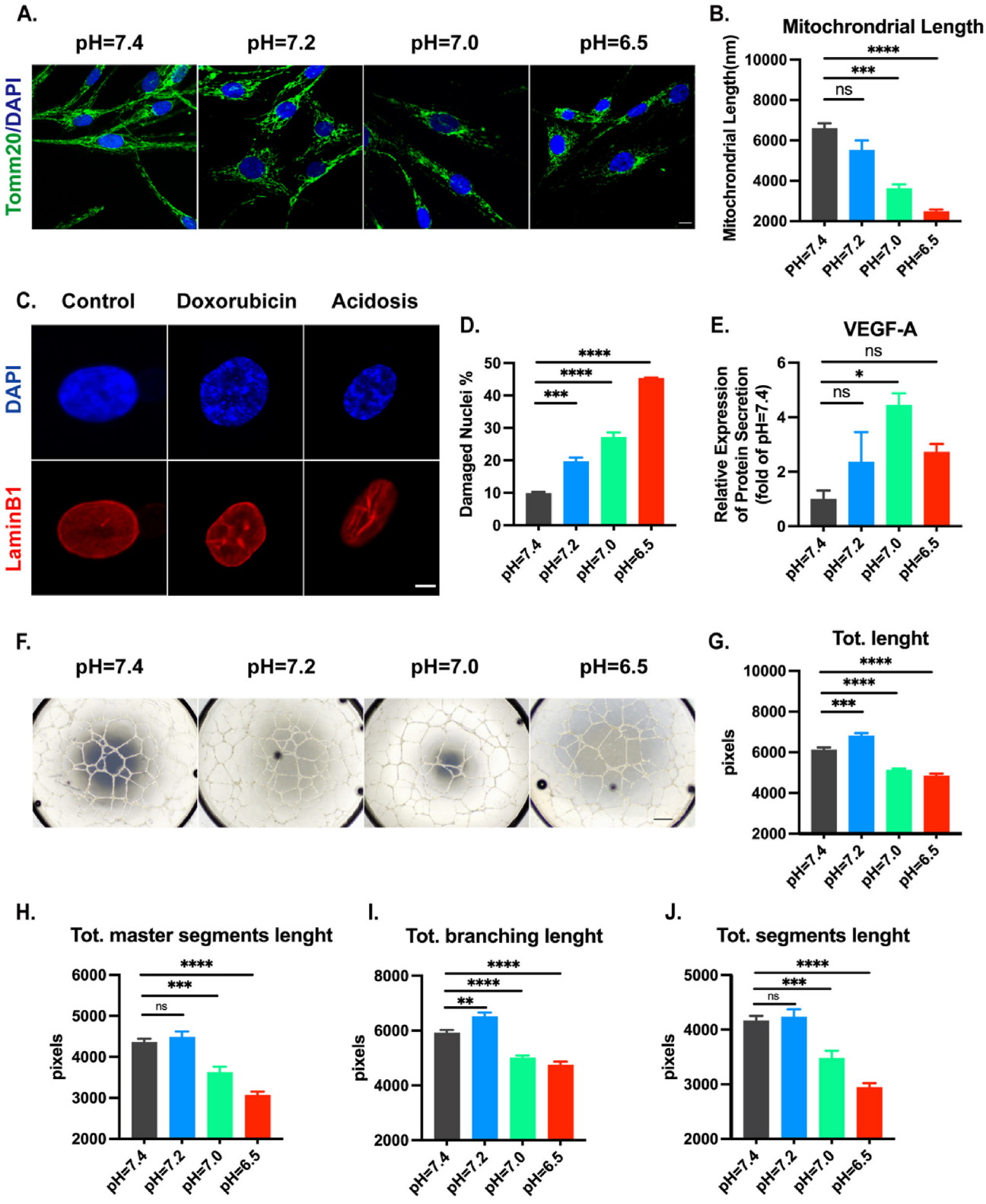

Fig. 3. Extracellular acidosis aggravated mitochondrial fragmentation and nuclear damage in ADSCs, impaired its contribution to angiogenesis in *vitro*. **(A)** The morphological changes of mitochondria induced by acidic treatments for 48 h Tomm20 (Green) and DAPI (blue) were used to label mitochondria and nucleus, respectively. Representative immunofluorescence staining was shown (scale bar = 10 μm). **(B)** The quantification of mitochondrial length control and experimental groups. **(C)** LAMIN B1 (red) and DAPI (blue) staining was performed to determine morphological characteristics of nuclei. Representative images of nuclear staining stimulated with doxorubicin and low pH were displayed (scale bar = 10 μm). **(D)**Nuclear membrane indentation and chromatin condensation in ADSCs were observed with exposure of DNA damage inducer and acidic pH. The percentage of cells with these morphological changes was used to quantify the nuclear damage in different acidic conditions. **(E–F)**. ADSCs were incubated with the culture medium at specific pH for 48 h. The culture medium was collected to determine the secreted protein level of vascular endothelial growth factor-A (VEGF-A) and effect on tube formation of human umbilical vein endothelial cells (HUVECs) (scale bar = 150 μm in F). **(G–J)** The quantification of total length **(G)**, total master segments length **(H)**, total branching length **(I)** and total segments length **(J)** was performed to evaluate angiogenesis in *vitro*. Data are presented as means ± SEM, *P < 0.05, **P < 0.01, ***P < 0.001, and ****P < 0.0001 by one-way ANOVA and Dunnett's post-hoc test.

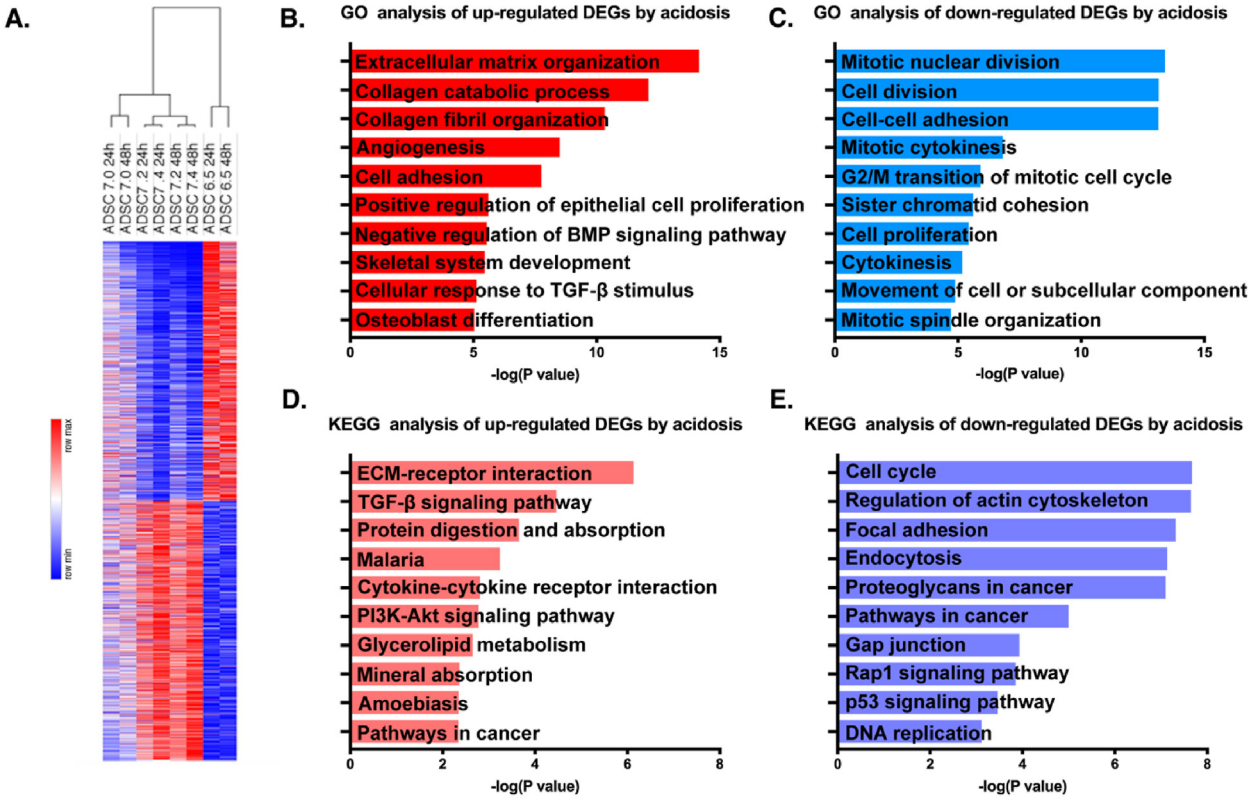

F.

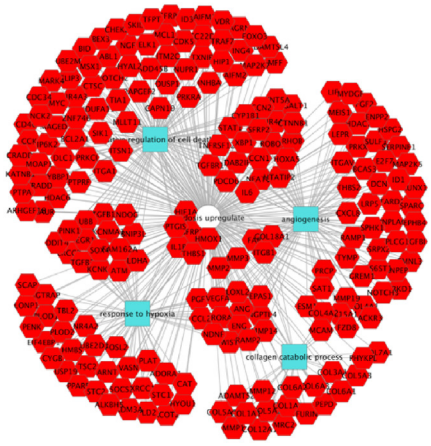

Gene Set	Node
Response to hypoxia	ACOT2, ADORA1, AGTRAP, ALKBH5 , ANG, ANGPTL4, ARNT, ATM, BNIP3L, CAT, CCL2, CYGB, DDIT4, EGR1, EIF4EBP1, ENDOG , ENG, EPAS1, ERCC3, FAM162A, FOSL2, HIF1A , HMBS, HMOX1, HYOU1, IL1B, KCNK2, KCNMA1, KDM3A, LDHA, LONP1, LOXL2 , MMP14, MMP2, NDNF, NR4A2, PENK, PGF, PINK1, PLAT, PLD2, PLOD1, PLOD2, PPARD, PTGIS, RAMP2, RORA, SCAP, SFRP1, SOCS3, SOX4, STC1, STC2, TBL2, TGFB1, TGFB3, THBS1, TSC2 , TWIST1 , UBB, UBE2D1, USP19, VASN, VEGFA , XRCC1
Collagen catabolic process	ADAMTS2, COL12A1, COL15A1, COL18A1, COL1A1, COL1A2, COL3A1, COL4A1, COL4A2, COL5A1, COL5A2, COL5A3, COL6A1, COL6A2, COL6A3, COL7A1, FAP, FURIN, ITGB1, MMP1, MMP12, MMP14, MMP19, MMP2, MMP3, MRC2, PEPD, PHYKPL
Angiogenesis	ACKR3, ANG, ANGPTL4, ANPEP, B4GALT1, BCAS3, CCL2, CCN1, CCN2, COL15A1, COL18A1, COL4A1, COL4A2, CTNNB1, CXCL8, CYP1B1, DAB2IP, DCN, E2F7, ENG, ENPP2, EPAS1, EPHB4, ESM1, FAP, FGF2, FMNL3, FZD8, GREM1, HDAC7, HIF1A , HMOX1, HOXA5, HS6ST1, HSPG2 , HTATIP2, ID1, IL1B, IL6, ITGAV, ITGB1, LEPR, LIF, LOXL2, LRP5, MAP2K5, MCAM , MEIS1, MMP14, MMP19, MMP2, MYDGF, NDNF, NFATC4, NOTCH3, NR4A1, PDCD6, PGF, PLCG1, PNPLA6, PRCP, PRKD1, PRKX, PTGIS, RAMP1, RAMP2, RHOB, ROBO1, RORA, RUNX1, SAT1, SERPINE1, SFRP1, SFRP2, SPARC, SPHK1, SRPX2, STARD13, STAT1, SULF1, TGFBI, TGFBR1, THBS1, THBS2, TNFRSF12A, TWIST1TYMP, VEGFA, WNT5A, XBP1
Positive regulation of cell death	ABL1, ADAMTSL4, AGRN, AIFM1, AIFM2, ARHGEF18, ATM, B4GALT1, BCL2A1, BEX3, BID, BNIP3L, CAPN10, CCK, CCN1, CCN2, CD40, CDC34 , CDK5, CHEK2, CLIP3, COL18A1, CRADD, CTNNB1, CTSC, CYP1B1, DAB2IP, DDIT4, DLC1, DUSP1, EGR1, ELK1, ENDOG, ERCC3, FAM162A, FAP, FOXO3, GADD45B, HDAC6, HIF1A, HIP1, HMOX1, HOXA5, HTATIP2, HYAL2 , ID3, IL1B, IL6, ING4, INHBA, IP6K2, ITGA1, ITGB1, ITM2C, ITSN1, KATNB1, KCNK2, KCNMA1, LDHA, MAGED1, MAP2K7, MARK4, MCL1, MFF, MLLT11, MMP2, MMP3, MOAP1, MSX1, MYBBP1A, MYC , NCK2, NDUFA13, NFATC4, NGF, NOTCH2, NR4A1, NR4A3 , NUPR1, PDCD6, PINK1, PLAUR, PRKCI, PRKRA, PTGIS , PTPA, PTPRF, RAPGEF2, RHOB, ROBO1, SFRP1, SFRP2, SFRP4, SIK1, SKIL, SOX4, STAT1, TFPT, TGFB1, TGFB3, TGFBR1, THBS1, TIA1, TNFRSF12A, TRADD, TRAF7, TSC22D1, TXNIP, UBB, UBE2M , VDR, WNT5A , XBP1, ZNF746

G.

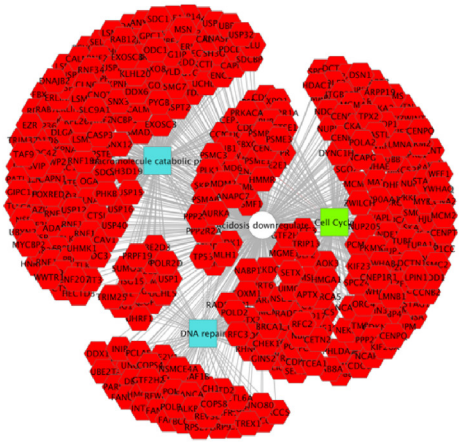

Gene Set	Node
Cell Cycle	ANAPC4, ANAPC7, ARPP19, AURKA, BIRC5, BLZF1, BRCA1, BRCC3, BUB1, BUB1B, CCNA2, CCNB1, CCNB2, CDC16, CDC20, CDC25B, CDC27, CDC6, CDC7, CDCA8, CDK1CDK5, RAP2, CDKN2C, CDKN2D, CENPA, CENPE , CENPF, CENPK, CENPM, CENPO, CENPQ, CENPT , CENPW, CEP192, CETN2, CHEK1, CKAP5, CNEP1R1, DCTN1, DCTN3, DHFR, DSN1, DYNC1H1, ENSA, FBXO5, FEN1, FOXM1, GINS2, GTSE1, H2AFX, H2AFZ, HDAC1, HMMR, HSP90AA1, ITGB3BP, KIF20A, KIF23, KIF2A, KNTC1, LIG1, LMNA , LMNB1, LPIN1, LPIN3, MAPK1, MAPRE1, MASTL, MAX, MCM2, MCM3 MCM4, MCM5, MCM6, MCM8, MDM2, MLH1, MYBL2, NBN, NCAPD2, NCAPG, NCAPG2, NCAPH2, NDC80, NDE1, NEDD1, NEK2, NSD2, NUF2, NUP153, NUP155, NUP205, NUP50, NUP54, NUP88, OPTN, ORC3, ORC4, PCBP4, PCM1, PCNA, PCNT, PHLDA1 , PKMYT1, PLK1, POLA2, POLD2, POLE, POLE3, PPP1CC, PPP1R12A , PPP2CB, PPP2R1A , PPP2R1B , PPP2R2A , PPP2R5A , PRKACA, PRKCA , PSMA6, PSMB10, PSMB9 , PSMC3 , PSMD14 , PSMD6, PSME1, PSME2, PSME3, PSMF1, RAB8A, RAD17, RAD50, RAD51C, RFC1, RFC2, RFC3 , RFC5, RHNO1, RPA1, RPA2, RRM2, SEM1, SGO2, SKA1, SKA2, SKP2, SMARCA5, SMC2, SMC3, SMC4, SPC24, SPC25, STAG1, STAG2, TFDP1, TMPO, TP53, TPR, TPX2, TUBA1A , TUBB, TUBB4B, TYMS, UBE2E1, UIMC1, VRK1, VRK2, WAPL, WEE1, WRAP53, XPO1, YWHAB YWHAE, YWHAH, YWHAQ, YWHAZ, ZW10, ZWILCH, ZWINT
DNA repair	ACTL6A, ALKBH3, APTX, ASCC3, ASF1A , BACH1, BCCIP, BRCA1, BRCC3, CDC14B, CDC7, CDK1, CDKN2D, CETN2, CHAF1B, CHEK1, COPS3, COPS4, COPS7A , COPS8, DDX1, DEK, DTL, DTX3L, ERCC5, FAN1, FANCA, FANCD2, FANCI, FEN1, FOXM1, GINS2, GTF2H1, GTF2H2, GTF2H3, H2AFX, HMGA1, HMGA2, HMGB2, INIP, INO80, INTS3, ISG15, LIG1, MCM8, MGME1, MLH1, MSH2, MUS81, NABP1, NBN, NSD2, NSMCE4A, PARP1, PARP3, PARP9, PCLAF, PCNA, PML , POLD2, POLE , POLH, POLR2D, POLR2L , PRKDC, PRPF19, PSMD14, RAD17, RAD50, RAD51AP1, RAD51C, RECQL, REV3L, RFC1, RFC2, RFC3, RFC5, RFWD3, RHNO1, RPA1, RPA2, RPS27L, SEM1, SETD2, SETX, SFR1, SIRT6, SLF2, SMARCA5 , SMC3, SMG1, SUMO3, TAOK3, TCEA1, TP53, TREX1, TRIM25, TRIP13, UBA7, UBE2D3, UBE2L6, UBE2T, UBE2V1, UCHL5, UHRF1, UIMC1, UNG, USP1, XRCC6
Macro-molecule catabolic process	ADAM9, AGO2, ANAPC4, ANAPC7, ANXA2, ATE1, AURKA, AZIN1, BUB1, BUB1B , CALM1, CALM2, CALM3, CAPN1, CAPN2, CASP3, CAST, CAV1, CCNB1, CD44, CD81, CDC16, CDC20, CDC27, CDC42, CDK1, CENPE, CENPF, CEP192, CLN5, CLN6, CLU, CNOT9, COPS3 , CTSK, CTSL, CYLD, DAB2, DDIT3, DDX6, DEDD, DLGAP5, DNAJB2, DTL, DYNC1LI1, ENC1, ERI1, ERLIN1, ERLIN2, EXOSC3, EXOSC8, EZR, FAF1, FAM83D, FBXL3 , FBXO11, FBXO31, FBXO5, FBXO8, FEN1, FLNA, FOXRED2, GIPC1, GPC1, GSK3B, GSPT2, GTSE1, GYG1, HECTD1, HECTD3, HMGB2, HMMR, HNRNPD, IDS, IGFBP3, ISG15, KCTD10, KLHL20, KLHL21, KPNA1, KPNB1, LSM1, LSM3, LSM5, LSM6, MDM2, MLH1, MSN, MUS81, MYCBP2, NCBP1, NFE2L2, NSF, ODC1, OGA, PATL1, PBK, PCYOX1, PDCD6IP, PDCL3, PHKB, PIK3R4, PLK1, PLK3, PML, POLR2D, PPP2CB, PPP2R1A , PPP2R2A , PRKACA , PRPF19 , PSMA6, PSMB10, PSMB9, PSMC3, PSMD14, PSMD6, PSME1 , PSME2 , PSME3, PSMF1, PTTG1IP, PYGB, RAB12, RAB7A , RDX, RNASEH2B, RNF115 , RNF139 , RNF14, RNF187, RNF19A, RNF20, RNF213 , RNF34, RNH1, RPL26L1 , SDC1, SDC2, SDC3, SDCBP, SEL1L, SH3D19, SH3GLB1, SKP2, SLC9A1, SMAD3, SMG1, SMG7, SMURF2, SNX12, SNX3, SUMO3, SVIP, TAF9, TATDN2, TLK2 , TOB1, TP53, TPR, TRIM25, TRIM32, UBA7, UBE2D3, UBE2E1, UBE2L3, UBE2L6 , UBR2, UBR3, UBXN2A, UBXN8, UCHL3, UCHL5, UHMK1, UHRF1, UPF2, USP1, USP12, USP13, USP14, USP15, USP16, USP24, USP25, USP32, USP40, USP48, USP5, WWP2, WWTR1, XPO1, ZFP36, ZMPSTE24, ZNF207, ZW10

fluorescent probes for visualizing cells at different cell cycle phase with different color. In this study, stable FUCCI system-expressed ADSCs in G1, G1/S, and S/G2/M displayed as red, yellow and green, respectively (Fig. 2F). Then we applied time-lapse imaging to record the cell cycle-dependent changes of fluorescence and a typical progression of cell cycle in ADSCs with control medium was shown (Supplementary Figure.S1). Initially, there was no obvious difference on the distribution of cell cycle before acidic treatments (Fig. 2G, H). After the exposure of low pH for 48 h, the population of G1 cells in pH 7.0 and 6.5 group was significantly enhanced in comparison with that in control group. In sharp contrast, the reduced percentage of G1/S and S/G2/M cells was observed at these groups (Fig. 2I), suggesting acidic environments induces the delay in cell cycle and suppress cell division. In line with that, flow cytometry analysis also revealed a G0/1 arrest and reduced frequency of cells in G2/M phase trigged by culture medium at pH 7.0 and 6.5 (Fig. 2J). Those results provide strong evidences that extracellular acidosis suppresses cell proliferation, induces cell apoptosis and cell cycle arrest in ADSCs using a pH-dependent manner.

3.3. Extracellular acidosis aggravated mitochondrial fragmentation and nuclear damage in ADSCs, impaired its contribution to angiogenesis in vitro

Mitochondrial dynamics play the pivotal role in stress/injury response and regenerative function of mesenchymal stem cells [35]. We thus explored the effect of extracellular acidosis on the mitochondrial fission and fusion of ADSCs. As shown in Fig. 3A, compared with the long and tubular mitochondrial networks determined by immunofluorescence staining of mitochondrial outer membrane (Tomm20) at control pH, the ones at low pH became much shorter and fragmented (Fig. 3B), which is associated with mitochondria impairment and apoptosis enhancement [36,37]. With further investigation**,** LaminB1 and DAPI staining were performed to observe the alteration of nuclear morphology. A well-known antitumor drug with cardiotoxicity, doxorubicin, which has been proved to induce cell cycle arrest and cell death via DNA damage in bone marrow mesenchymal stem cells (BM-MSCs) [38], was used to stimulate ADSCs as DNA damage inducer (15 μM) here. In the control group, culture cells had rounded and intact nuclear membranes, however, cells undergoing nuclear indentations and chromatin condensation were observed in the present of acidosis and doxorubicin (Fig. 3C). The percentage of cells with those morphological changes was increased following a decreased pH (Fig. 3D), indicating that acidic conditions induce nuclear damage in a pH-dependent way. Paracrine secretion is the most important mechanism in therapeutic angiogenesis of ADSCs transplant for ischemic diseases. To investigated the role of acidic environment in angiogenetic factor secretion from ADSCs and the interaction between endothelial cells and ADSCs, culture medium was collected after 48 h-incubation with the specific pH in ADSCs. Based on Elisa detecting, a stimulated VEGF-A secretion from ADSCs was observed at the condition of pH 7.0, while the effect was attenuated at the lowest of pH (Fig. 3E). We next used the culture medium to treat HUVECs for tube formation evaluation (Fig. 3F). It's interesting to note that medium from the mild pH group promotes the endothelial tube formation assessed by total length, total master segments length, total branching length and total segments length (Fig. 3G–J), however, the collected medium from pH 7.0 and 6.5 group remarkably impaired the ability of tube formation in spite of the increased level of VEGF-A protein in that. Taken together, these observations demonstrate that acidosis induces disorder of mitochondrial dynamics and nuclear damage in ADSCs, and also impairs its proangiogenic effect *in vitro*.

3.4. Acidosis-driven genes and pathways in ADSCs

To determine the transcriptional changes induced by acidosis in ADSCs, we performed the RNA-sequencing analysis of cells exposed with different acidic environment for 24 and 48 h. DEGs between low pH (pH = 7.2/7.0/6.5) and control groups (pH = 7.4) were screened with a threshold of $\log_2$FoldChange $\geq$1.0 as well as false discovery rate (FDR) $\leq$0.001, and then subjected for clustering analysis (Fig. 4A). The results of volcano plots and venn diagrams analysis revealed that transcriptional changes depend on the pH level mainly (Supplementary Figure. S2 A-B). Next, the GO term analysis revealed that the up-regulated DEGs trigged by acidosis are mainly involved extracellular matrix organization, collagen catabolism and angiogenesis, whereas the down-regulated genes are mostly related to cell division, cell cycle as well as cell proliferation (Fig. 4B, C). In line with that, KEGG pathway profiling showed that the most upregulated genes are connected with extracellular matrix (ECM)-receptor interaction, TGF-β signaling pathway, and inflammation activating pathway, while the down-regulated genes are largely enriched in cell cycle, actin cytoskeleton regulation, endocytosis together with cancer-related pathways (Fig. 4D, E). Furthermore, to have a better understanding of molecular interactions affected by extracellular acidosis, the PPI network enrichment analysis was subjected. DEGs were input to the ToppCluster online tool and a 0.05 p-value cutoff with Bonferroni test was set for functional enrichment analysis. Pathways and gene ontology features were applied for the enrichment of gene modules. Gene enrichment score (-$\log_{10}$ p value) was used to evaluate the power of association between gene modules and the top modules were selected to generate the interaction networks. We identified that the most up-regulated modules were linked to the response to hypoxia, collagen catabolic process, angiogenesis, and positive regulation of cell death (Fig. 4F), and the most down-regulated modules were related to the cell cycle, DNA repair and macromolecule catabolic process (Fig. 4G). All genes in those modules were listed as right. Based on the observed phenotypes on cell proliferation, cell cycle and DNA damage in ADSCs exposed with acidosis, we thus further examined the genes expressions linking these pathways. Consistent with the data of cell experiments, acidic conditions suppressed expressions of DNA repair, DNA replication, cell cycle-relative genes, and accelerated the expression level of genes associated with senescence (Fig. 5A), reflecting that alternative mechanisms and damages of DNA processes had been triggered before cell death. Our observations, combined with the results from cell examinations, suggest that extracellular acidosis triggers cell cycle arrest, disorder of collagen metabolism, senescence progression, DNA damage and cell death enhancement.

Fig. 4. Key genes and pathways regulated with acidic pH in ADSCs. **(A)** RNA-Sequencing analysis was performed in ADSCs stimulated with the indicated pH condition for 24 h and 48 h. Clustering analysis of differentially expressed genes (DEGs) from control and experimental groups. **(B–E)** Gene ontology (GO) and Kyoto encyclopedia of genes and genomes (KEGG) enrichment analysis of DEGs with up-regulation and down-regulation. **(F–G)** Protein–protein interaction (PPI) network enrichment analysis showed the relationship of acidosis-related gene modules using ToppCluster online tool. The most up-regulated gene modules conducted by acidic conditions were connected with response to hypoxia, collagen catabolic process, angiogenesis and positive regulation of cell death **(F)**. The most down-regulated gene modules induced by low pH conditions were related to cell cycle, DNA repair and macromolecule catabolic process mainly **(G)**. The relative genes of these modules were listed on right.

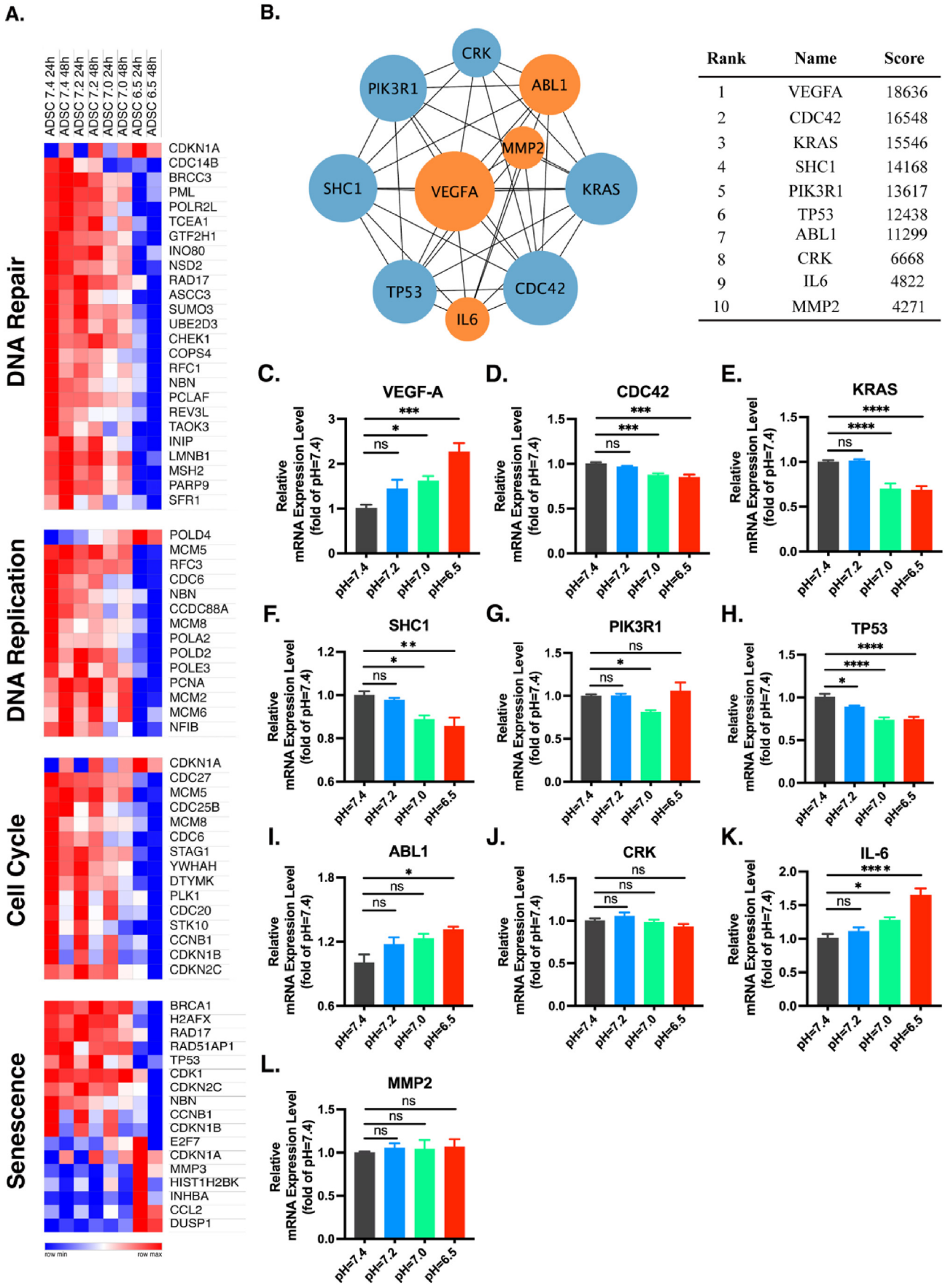

Rank	Name	Score
1	VEGFA	18636
2	CDC42	16548
3	KRAS	15546
4	SHC1	14168
5	PIK3R1	13617
6	TP53	12438
7	ABL1	11299
8	CRK	6668
9	IL6	4822
10	MMP2	4271

3.5. Identification of hub genes for extracellular acidosis in ADSCs

To research genes interaction and identify the hub genes of acidic pH regulation in ADSCs, a PPI network including 441 nodes and 1170 edges was constructed with search tool for the retrieval of interacting genes (STRING) online database. Using Cytoscape software and cytohubba plug-in, the top 10 hub genes were selected with maximal clique centrality (MCC) score (Fig. 5B). The genes with up-regulation and down-regulation were displayed as orange and blue circles, respectively. To further confirm the results from bioinformatics analysis, we used qRT-PCR to determine the transcriptional changes of these hub genes (Fig. 5C–L). Except for CRK proto-oncogene, adaptor protein (CRK, also known as p38) and matrix metallopeptidase 2 (MMP2), the enhanced mRNA expression of VEGF-A, ABL proto-oncogene 1, non-receptor tyrosine kinase (ABL1) and interleukin 6 (IL-6) together with the reduced gene expressions of cell division cycle 42 (CDC42), KRAS proto-oncogene, GTPase (KRAS), SHC adaptor protein 1(SHC1), phosphoinositide-3-kinase regulatory subunit 1(PIK3R1) and tumor protein p53 (TP53) were noted in ADSCs with low pH stimulations, which was in accord with the findings from RNA-sequencing. Collectively, these results identify and validate hub gens of extracellular acidosis in ADSCs, suggesting treatments aimed at those genes may have therapeutic potential in acidic conditions for ADSC-based therapy.

4. Discussion

In view of high morbidity and mortality in CLI, novel therapies need to be developed urgently for patients who are ineligible for endovascular treatment and surgical bypass [39,40]. In comparison with gene therapy and sole growth factor stimulation, there are obvious advantages of stem cell-based strategy such as multiple capacities of differentiation and paracrine effects [41]. Thus, stem cell-based therapies are promising and some of them have been proved to promote angiogenesis effectively in ischemic conditions [11]. Notably, ADSCs display an outstanding prospect for angiogenic therapies with stem cells based on their sufficient donor sources, multidifferentiation potential, powerful paracrine secretion and immune system modulation [42,43]. However, many researches didn't provide sufficient evidences to show clinical benefits on outcomes in CLI patients, which are pivotal to become a regular clinical treatment for stem cell-based therapies [11]. In this case, reasons underlying the limited function of transplanted stem cells need to be explored urgently. Tissue acidosis is a common characteristic feature in various pathological conditions including ischemia, inflammation, as well as tumor [44]. In this study, we investigated the possibility that the acidic environment of ischemic tissues negatively affects ADSCs function and survival. The metabolic acidosis of ischemic limbs in our mouse model was verified by an increased concentration of lactate, which is highly sensitive marker for the metabolic state in tissues [45,46]. Hypoxia results in anaerobic glycolysis, which produces the lactate with H^+, leading to lactate accumulation and lowering the extracellular pH [47]. Thus, lactate concentration reflects the pH of the environment partly. In this setting, we observed an elevated concentration of lactate at first 30 min after induction of ischemia and the concentration remained elevated for 72 h. Especially, lactate concentration reached the peak level at 24 h after femoral artery occlusion, suggesting that there are other elements promoting lactate generation at this time point. One of these could be inflammation, as it has been reported that gene expression of many inflammatory cytokines peaks during the 6–24 h period of ischemia [48]. Moreover, we also measured the continuous changes of glucose level in the ischemic tissues. Interestingly, it has been reported that the glucose concentration in the back muscles of rats is unaffected by a 30 min hypoxic exposure [27]. But, in our observation, the down-regulation of glucose level was determined at the first 30 min of ischemia. During 0.5–72 h of post-ischemia, there was a persistent decline in extracellular glucose concentration in the ischemic tissues, reflecting the imbalanced energy metabolism and glucose exhaustion triggered by ischemia.

Considering the likely heterogeneity between CLI patients in terms of the pH in ischemic tissues, we explored the effect of acidosis ranging from pH 7.4 to 6.5 on ADSCs for experiments *in vitro*. Previous studies have shown that acidic microenvironment can inhibit cell proliferation [25,49]. In accord, our data confirmed that acidic conditions suppress cell proliferation and cell viability using a pH-dependent manner with $Ki67^+$ index evaluation and cell viability assay. For cell apoptosis, our results diverged from previous studies. One study suggested that cell apoptosis could be induced by an acidic exposure lasting as little as 30 s, in a time- and pH-dependent way [22]. However, another study suggested that 24 h exposure of acidic pH reduces cell apoptosis and promotes anti-apoptotic gene expression [25]. Therefore, we used two different methods including annexin V^+ staining and caspase 3/7 activation to detect the effect of acidosis on cell apoptosis. In the present study, both of these indicated that acidic conditions have no significant effect on apoptosis in ADSCs except at pH of 6.5. These observations can explain partly the poor survival of transplanted cells in ischemic areas [21].

With cell cycle reporter FUCCI system and PI staining, we found that acidic medium at pH 7.0 and 6.5 for 48 h induced an obvious G1 arrest and cell division inhibition in ADSCs, which was in line with the observed proliferation limitation. In the previous report, chromatin condensation was regarded as an DNA damage indicator, at the same time, nuclear indentation was believed to reflect senescent progression, even though the exact molecular mechanisms of them remain to be fully investigated [50]. Here, we demonstrated the percentage of ADSCs with chromatin condensation and nuclear indentation is increased following a decrease of pH, indicating that extracellular acidosis induces nuclear damage using a pH-dependent way. In addition, Tomm20 staining showed the reduced mitochondrial length and more fragmented mitochondria with uneven distribution in the presence of low pH. Mitochondrial morphology depends on the equilibrium between organelle fusion and fission [51], and it has been shown that fragmented mitochondria are related to apoptosis and small round mitochondria could be detected at the very early stages of cell death [52]. Therefore, our studies suggested that the alteration of mitochondrial dynamics observed in this experiment may reflect early apoptosis promoted by acidosis.

VEGF-A plays a crucial role of angiogenic processes in physiological and pathological conditions [53]. Extracellular acidosis has been identified to promote VEGF-A expression in cancer cells [54]. In support of this, the expression of VEGF-A was enhanced significantly at both of mRNA and protein level in ADSCs with acidic exposures. It's interesting to note that the conditional medium from mild pH group promotes the endothelial tube formation, whereas the increased VEGF-A protein secretion and transcription in conditional medium from pH 7.0 and 6.5 group leads to the

Fig. 5. Gene alteration of pivotal biological processes and hub genes induced by acidosis. **(A)** Heatmap presented the acidic condition-induced gene modification in DNA repair, DNA replication, cell cycle and senescence. **(B)** The top 10 hub genes in response extracellular acidosis were screened by cytohubba plug-in and listed with their respective maximal clique centrality (MCC) score. The orange and blue circles represent genes with up-regulation and down-regulation. **(C–L)** The identification of hub genes via qRT-PCR. Data are presented as means ± SEM, *P < 0.05, **P < 0.01, ***P < 0.001, and ****P < 0.0001 by one-way ANOVA and Dunnett's post-hoc test.

angiogenic inhibition *in vitro*. Whether the enhanced VEGF-A expression represents a feedback of impairment rather than angiogenic function promotion remains unknown. One possible could be that the acidic pH impairs endothelial function in response to VEGF-A in HUVECs [55]. Another possibility is hypoxia-inducible factor 1α (HIF-1α), a pivotal promoter for the transcription of VEGF-A [56], the increased expression of HIF-1α triggered by acidosis in ADSCs was also confirmed with RNA-sequencing and qRT-PCR (data not shown). In any case, our date determined that ADSCs with mild pH exposure promotes endothelial function, however, the angiogenic effect of ADSCs is remarkably impaired by severe extracellular acidosis.

In the transcriptomic analysis, the up-regulated pathways responsive to acidosis significantly are extracellular matrix organization and transforming growth factor β (TGF-β) signaling pathway. Extracellular matrix organization and collagen have been identified to be increased in acidosis and bone metastasis of breast cancer cells [57], while there is another study pointed out that acidosis damages the synthesis and secretion of extracellular matrix proteins in BM-MSCs [58]. Thus, the contribution of extracellular matrix organization in ADSCs transplanting with acidic environment remains to be investigated. In the other hand, it is not surprising to note that up-regulated DEGs are largely enriched in TGF-β pathway, as its great importance in tissue repair after ischemic injury [59]. Importantly, we found that genes in modules of response to hypoxia and angiogenesis are up-regulated obviously. The earlier study has revealed that tissue oxygen partial pressure and pH regulate the VEGF transcription though their respective pathways in human glioma cells [60]. In contrast, our results showed that low pH induces hypoxia directly in ADSCs, however, VEGF-A-mediated endothelial response is suppressed by severe acidic conditions. Likewise, we determined that cell cycle is the one of most down-regulated pathways in response to acidosis, and genes in pathway of DNA repair and DNA replication are also inhibited by acidic stimulations. These data fit well with phenotypes we observed from cell experiments. Based on the clue from increased nuclear impairment, we noted the transcriptional changes on senescence-related genes including cyclin dependent kinase inhibitor 1 A (CDKN1A, also known as P21) and E2F transcription factor 7 (E2F7) [61], reflecting that extracellular acidification promotes the progression of cell senescence.

Programmed cell death is an important defense to maintain homeostatic balance under detrimental conditions [62]. In this study, we also observed a loss of p53 function and mitotic cell cycle checkpoint followed by impaired DNA repair in ADSCs with acidic exposures, which is critical for senescence stem cells to transform into cancer stem cells if they escape cell death [62,63]. Hence, our findings suggested the risk of tumorigenicity when the number of transplanted cells is large in an acidic microenvironment.

In addition, we also screened top 10 hub genes for acidosis-mediated effects on ADSCs. Using qRT-PCR, the expression of VEGF-A, ABL1, IL-6, CDC42, KRAS, SHC1, together with PIK3R1 and TP53 was identified to be consistent with bioinformatics analysis. Among them, ABL1 is well-known as a protooncogene. The fusion between ABL1 and breakpoint cluster region (BCR) was mainly related to chronic myeloid leukemia (CML) and B-cell acute lymphoblastic leukemia (ALL) [64]. IL-6 plays a typical cytokine in the immune regulation against tissue damages. However, the excessive expression of IL-6 results in an aggravated inflammation response [65]. The increased serum level of IL-6 has been identified to be associated with metabolic acidosis in hemodialysis patients. Also, pre-clinical research showed that the up-regulated IL-6 secreted from myocardium is observed in rats with chronic acidosis [66,67]. CDC42 is a small GTPase involved in a great number of biological regulations. Recent studies have indicated that the dysregulation of CDC42 caused aging in somatic and stem cells, and lead to age-related diseases such as neurodegenerative and cardiovascular dysfunctions [68,69]. KRAS is also an oncogene, the mutations of KRAS are involved in many different kinds of tumors [70]. Interestingly, both SHC1 and PIK3R1 are adapter proteins. Several evidences determined that the formation of multiprotein complex containing SHC1, PIK3R1 and other G proteins is response to 17β-estradiol (E2) stimulation in breast cancer cells, which supports cancer cell proliferation and suppressed apoptosis [71]. The known information suggests some meaningful clues, however, the impacts of those hub gens on acidosis for ADSCs-based therapy remain to be explored.

There are some limitations in this study should be considered. The local pH in ischemic tissues after blood flow occlusion need to be measured. We tested the local pH in hindlimb muscles using pH probe, however, the pH valves were not stable and accurate during the detecting period. Thus, we believe more precise equipment should be performed for pH measurement. Since the deleterious effect of acidosis on ADSCs is pH-dependent mainly, it will be good to know the specific pH to determine therapeutic strategy basing on ADSCs transplanting. Additionally, metabolic alteration triggered by acidosis remains unclear, more pro-clinical and clinical researches are required to indicate the metabolic pathways in acidic conditions.

5. Conclusions

In sum, our study determines the lactic and glucose level in hindlimb muscles during 0.5–72 h of post-ischemia by microdialysis and characterizes the impacts of extracellular acidosis on ADSCs *in vitro*. Acidosis induces restricted proliferation, obvious cell apoptosis and cell cycle arrest, at the same time, it also results in mitochondrial dynamics disorder, DNA damage, impairment of proangiogenic function as well as senescence aggravation in a pH-dependent manner, leading to the limited function of stem cell-based therapy. These findings suggest that the balance of tissue pH might improve the effectiveness of ADSCs transplanting and treatments focus on acidosis-mediated hub genes may have therapeutic potential in clinical application.

Data availability

Our data are available on reasonable requests to the corresponding authors.

Funding

This work was supported by National Natural Science Foundation of China grant 82120108004 (Dr. Liang) and 82100479 (Dr. Chen), and Shanghai Sailing Program grant 21YF1458300 (Dr. Chen). The authors received financial supports for the research and publication of this article.

Declaration of competing interest

The authors declare that they have no conflicts of interest with the contents of this article. Every author agrees with to being listed as an author and the submission to regenerative therapy.

Appendix A. Supplementary data

Supplementary data to this article can be found online at https://doi.org/10.1016/j.reth.2024.01.010.

References

[1] Abu Dabrh AM, Steffen MW, Undavalli C, Asi N, Wang Z, Elamin MB, et al. The natural history of untreated severe or critical limb ischemia. J Vasc Surg 2015;62:1642–1651 e1643.
[2] Bradbury A, Ruckley C, Fowkes F, Forbes J, Gillespie I, Adam DJL. Bypass versus angioplasty in severe ischaemia of the leg (BASIL): multicentre, randomised controlled trial 2005;366:1925–34.
[3] Norgren L, Hiatt WR, Dormandy JA, Nehler MR, Harris KA, Fowkes FGR. Inter-society consensus for the management of peripheral arterial disease (TASC II). J Vasc Surg 2007;45:S5–67.
[4] Fujita Y, Kawamoto A. Stem cell-based peripheral vascular regeneration. Adv Drug Deliv Rev 2017;120:25–40.
[5] Becker F, Robert-Ebadi H, Ricco J-B, Setacci C, Cao P, De Donato G, et al. Chapter I: definitions, epidemiology, clinical presentation and prognosis. Eur J Vasc Endovasc Surg 2011;42:S4–12.
[6] Zheng Y, Qin J, Wang X, Peng Z, Hou P, Lu X. Dynamic imaging of allogeneic adipose-derived regenerative cells transplanted in ischemic hind limb of apolipoprotein E mouse model. Int J Nanomed 2017;12:61.
[7] Nakagami H, Maeda K, Morishita R, Iguchi S, Nishikawa T, Takami Y, et al. Novel autologous cell therapy in ischemic limb disease through growth factor secretion by cultured adipose tissue–derived stromal cells. Arterioscler Thromb Vasc Biol 2005;25:2542–7.
[8] Fan W, Sun D, Liu J, Liang D, Wang Y, Narsinh KH, et al. Adipose stromal cells amplify angiogenic signaling via the VEGF/mTOR/Akt pathway in a murine hindlimb ischemia model: a 3D multimodality imaging study. PLoS One 2012;7:e45621.
[9] Eto H, Suga H, Matsumoto D, Inoue K, Aoi N, Kato H, et al. Characterization of structure and cellular components of aspirated and excised adipose tissue. Plast Reconstr Surg 2009;124:1087–97.
[10] Cherubino M, Rubin JP, Miljkovic N, Kelmendi-Doko A, Marra KG. Adipose-derived stem cells for wound healing applications. Ann Plast Surg 2011;66:210–5.
[11] Shirbaghaee Z, Hassani M, Heidari Keshel S, Soleimani M. Emerging roles of mesenchymal stem cell therapy in patients with critical limb ischemia. Stem Cell Res Ther 2022;13:1–25.
[12] Badillo AT, Redden RA, Zhang L, Doolin EJ, Liechty KW. Treatment of diabetic wounds with fetal murine mesenchymal stromal cells enhances wound closure. Cell Tissue Res 2007;329:301–11.
[13] Blanton MW, Hadad I, Johnstone BH, Mund JA, Rogers PI, Eppley BL, et al. Adipose stromal cells and platelet-rich plasma therapies synergistically increase revascularization during wound healing. Plast Reconstr Surg 2009;123:56S–64S.
[14] Ebrahimian TG, Pouzoulet F, Squiban C, Buard V, André M, Cousin B, et al. Cell therapy based on adipose tissue-derived stromal cells promotes physiological and pathological wound healing. Arterioscler Thromb Vasc Biol 2009;29:503–10.
[15] Rehman J, Traktuev D, Li J, Merfeld-Clauss S, Temm-Grove CJ, Bovenkerk JE, et al. Secretion of angiogenic and antiapoptotic factors by human adipose stromal cells. Circulation 2004;109:1292–8.
[16] Procházka V, Gumulec J, Jalůvka F, Šalounová D, Jonszta T, Czerný D, et al. Cell therapy, a new standard in management of chronic critical limb ischemia and foot ulcer. Cell Transplant 2010;19:1413–24.
[17] Teraa M, Sprengers RW, Schutgens RE, Slaper-Cortenbach IC, Van Der Graaf Y, Algra A, et al. Effect of repetitive intra-arterial infusion of bone marrow mononuclear cells in patients with no-option limb ischemia: the randomized, double-blind, placebo-controlled JUVENTAS trial. Circulation 2015;131:114.012913. CIRCULATION AHA.
[18] Weem SP, Teraa M, De Borst G, Verhaar M, Moll F. Bone marrow derived cell therapy in critical limb ischemia: a meta-analysis of randomized placebo controlled trials. Eur J Vasc Endovasc Surg 2015;50:775–83.
[19] Capoccia BJ, Robson DL, Levac KD, Maxwell DJ, Hohm SA, Neelamkavil MJ, et al. Revascularization of ischemic limbs after transplantation of human bone marrow cells with high aldehyde dehydrogenase activity. Blood 2009;113:5340–51.
[20] Losordo DW, Dimmeler S. Therapeutic angiogenesis and vasculogenesis for ischemic disease: part II: cell-based therapies. Circulation 2004;109:2692–7.
[21] Qadura M, Terenzi DC, Verma S, Al-Omran M, Hess DA. Concise review: cell therapy for critical limb ischemia: an integrated review of preclinical and clinical studies. Stem Cell 2018;36:161–71.
[22] D'atri LP, Etulain J, Romaniuk MA, Torres O, Negrotto S, Schattner MJT. The low viability of human CD34+ cells under acidic conditions is improved by exposure to thrombopoietin, stem cell factor, interleukin-3, or increased cyclic adenosine monophosphate levels 2011;51:1784–95.
[23] O'Donnell TF, Raines JK, Darling RC. Relationship of muscle surface pH to noninvasive hemodynamic studies. Arterial Occlusive Dis 1979;114:600–4.
[24] Hamm LL, Nakhoul N, Hering-Smith KS. Acid-base homeostasis. Clin J Am Soc Nephrol 2015;10:2232–42.
[25] Massa A, Perut F, Chano T, Woloszyk A, Mitsiadis T, Avnet S, et al. The effect of extracellular acidosis on the behaviour of mesenchymal stem cells in vitro. Eur Cell Mater 2017;33:252–67.
[26] Limbourg A, Korff T, Napp LC, Schaper W, Drexler H, Limbourg FP. Evaluation of postnatal arteriogenesis and angiogenesis in a mouse model of hind-limb ischemia. Nat Protoc 2009;4:1737–48.
[27] Zoremba N, Homola A, Rossaint R, Syková E. Interstitial lactate, lactate/pyruvate and glucose in rat muscle before, during and in the recovery from global hypoxia. Acta Veter Scand 2014;56:72.
[28] Valtysson J, Persson L, Hillered L. Extracellular ischaemia markers in repeated global ischaemia and secondary hypoxaemia monitored by microdialysis in rat brain. Acta Neurochir (Wien) 1998;140:387–95.
[29] Müller M. Science, medicine, and the future: microdialysis. BMJ 2002;324:588.
[30] Koh S-B, Mascalchi P, Rodriguez E, Lin Y, Jodrell DI, Richards FM, et al. A quantitative FastFUCCI assay defines cell cycle dynamics at a single-cell level. J Cell Sci 2017;130:512–20.
[31] Kong LY, Liang C, Li PC, Zhang YW, Feng SD, Zhang DH, et al. Myotubularin-related Protein14 prevents neointima formation and vascular smooth muscle cell proliferation by inhibiting polo-like Kinase1. J Am Heart Assoc 2022;11:e026174.
[32] Langmead B, Salzberg SL. Fast gapped-read alignment with Bowtie 2. Nat Methods 2012;9:357.
[33] Li B, Dewey CN. RSEM: accurate transcript quantification from RNA-Seq data with or without a reference genome. BMC Bioinf 2011;12:323.
[34] Böhme I, Bosserhoff A. Extracellular acidosis triggers a senescence-like phenotype in human melanoma cells. Pigment Cell Melanoma Res 2020;33:41–51.
[35] Ren L, Chen X, Chen X, Li J, Cheng B, Xia J. Mitochondrial dynamics: fission and fusion in fate determination of mesenchymal stem cells. Front Cell Dev Biol 2020;8:580070.
[36] Shaughnessy DT, McAllister K, Worth L, Haugen AC, Meyer JN, Domann FE, et al. Mitochondria, energetics, epigenetics, and cellular responses to stress. Environ Health Perspect 2014;122:1271–8.
[37] Ma L, Feng X, Wang K, Song Y, Luo R, Yang C. Dexamethasone promotes mesenchymal stem cell apoptosis and inhibits osteogenesis by disrupting mitochondrial dynamics. FEBS Open Bio 2020;10:211–20.
[38] Cruet-Hennequart S, Prendergast ÁM, Shaw G, Barry FP, Carty MP. Doxorubicin induces the DNA damage response in cultured human mesenchymal stem cells. Int J Hematol 2012;96:649–56.
[39] Criqui MH, Aboyans V. Epidemiology of peripheral artery disease. Circ Res 2015;116:1509–26.
[40] Hess CN, Norgren L, Ansel GM, Capell WH, Fletcher JP, Fowkes FGR, et al. A structured review of antithrombotic therapy in peripheral artery disease with a focus on revascularization: a TASC (InterSociety Consensus for the Management of Peripheral Artery Disease) initiative. Circulation 2017;135:2534–55.
[41] Beltrán-Camacho L, Rojas-Torres M, Durán-Ruiz MC. Current status of angiogenic cell therapy and related strategies applied in critical limb ischemia. Int J Mol Sci 2021;22:2335.
[42] Lu H, Wang F, Mei H, Wang S, Cheng L. Human adipose mesenchymal stem cells show more efficient angiogenesis promotion on endothelial colony-forming cells than umbilical cord and endometrium. Stem Cell Int 2018;2018.
[43] Zhao L, Johnson T, Liu D. Therapeutic angiogenesis of adipose-derived stem cells for ischemic diseases. Stem Cell Res Ther 2017;8:1–9.
[44] Riemann A, Wußling H, Loppnow H, Fu H, Reime S, Thews O. Acidosis differently modulates the inflammatory program in monocytes and macrophages. Biochim Biophys Acta (BBA) Mol Basis Dis 2016;1862:72–81.
[45] Behrens P, Langemann H, Strohschein R, Draeger J, Henning JJ. Extracellular glutamate and other metabolites in and around RG2 rat glioma: an intracerebral microdialysis study. J Neuro Oncol 2000;47:11–22.
[46] Serganova I, Rizwan A, Ni X, Thakur SB, Vider J, Russell J, et al. Metabolic imaging: a link between lactate dehydrogenase A, lactate and tumor phenotype. Clin Cancer Res 2011. 0397.2011.
[47] Kraut JA, Madias NE. Lactic acidosis. N Engl J Med 2014;371:2309–19.
[48] Petersen AH, van Luyn MJA, Rozenbaum MH, Vandervelde S, Harmsen MC, Tio RA. Stem cell-related cardiac gene expression early after murine myocardial infarction. Cardiovasc Res 2007;73:783–93.
[49] Mena HA, Lokajczyk A, Dizier B, Strier SE, Voto LS, Boisson-Vidal C, et al. Acidic preconditioning improves the proangiogenic responses of endothelial colony forming cells. Angiogenesis 2014;17:867–79.
[50] Chandra T, Kirschner K, Thuret J-Y, Pope BD, Ryba T, Newman S, et al. Independence of repressive histone marks and chromatin compaction during senescent heterochromatic layer formation. Mol Cell 2012;47:203–14.
[51] MacVicar T, Langer T. OPA1 processing in cell death and disease–the long and short of it. J Cell Sci 2016;129:2297–306.
[52] Karbowski M, Youle RJ. Dynamics of mitochondrial morphology in healthy cells and during apoptosis. Cell Death Differ 2003;10:870.
[53] Ferrara N, Gerber H-P, LeCouter J. The biology of VEGF and its receptors. Nat Med 2003;9:669–76.
[54] Shi Q, Le X, Wang B, Abbruzzese JL, Xiong Q, He Y, et al. Regulation of vascular endothelial growth factor expression by acidosis in human cancer cells. Oncogene 2001;20:3751–6.
[55] Faes S, Uldry E, Planche A, Santoro T, Pythoud C, Demartines N, et al. Acidic pH reduces VEGF-mediated endothelial cell responses by downregulation of VEGFR-2; relevance for anti-angiogenic therapies. Oncotarget 2016;7:86026.
[56] Otrock ZK, Mahfouz RA, Makarem JA, Shamseddine AI. Understanding the biology of angiogenesis: review of the most important molecular mechanisms. Blood Cell Mol Dis 2007;39:212–20.
[57] Yamagata AS, Freire PP, Jones Villarinho N, Teles RHG, Francisco KJM, Jaeger RG, et al. Transcriptomic response to acidosis reveals its contribution to bone metastasis in breast cancer cells. Cells 2022;11:544.

[58] Massa A, Perut F, Chano T, Woloszyk A, Mitsiadis TA, Avnet S, et al. The effect of extracellular acidosis on the behaviour of mesenchymal stem cells in vitro. Eur Cell Mater 2017;33:252–67.
[59] Chen H, Li D, Saldeen T, Mehta JL. TGF-β1 attenuates myocardial ischemia-reperfusion injury via inhibition of upregulation of MMP-1. Am J Physiol Heart Circ Physiol 2003;284:H1612–7.
[60] Fukumura D, Xu L, Chen Y, Gohongi T, Seed B, Jain RK. Hypoxia and acidosis independently up-regulate vascular endothelial growth factor transcription in brain tumors in vivo. Cancer Res 2001;61:6020–4.
[61] Qian Y, Chen X. Senescence regulation by the p53 protein family. Cell Senescence 2013:37–61. Springer.
[62] Fuchs Y, Steller H. Programmed cell death in animal development and disease. Cell 2011;147:742–58.
[63] Nassour J, Radford R, Correia A, Fusté JM, Schoell B, Jauch A, et al. Autophagic cell death restricts chromosomal instability during replicative crisis. Nature 2019;565:1.
[64] De Braekeleer E, Douet-Guilbert N, Rowe D, Bown N, Morel F, Berthou C, et al. ABL1 fusion genes in hematological malignancies: a review. Eur J Haematol 2011;86:361–71.
[65] Tanaka T, Narazaki M, Kishimoto T. Interleukin (IL-6) immunotherapy. Cold Spring Harbor Perspect Biol 2018;10:a028456.
[66] Zahed NS, Chehrazi S. The evaluation of the relationship between serum levels of Interleukin-6 and Interleukin-10 and metabolic acidosis in hemodialysis patients. Saudi J Kidney Dis Transplant 2017;28:23–9.
[67] Lasheen NN, Mohamed GF. Possible mechanisms of cardiac contractile dysfunction and electrical changes in ammonium chloride induced chronic metabolic acidosis in Wistar rats. Physiol Res 2016;65:927.
[68] Umbayev B, Safarova Y, Yermekova A, Nessipbekova A, Syzdykova A, Askarova S. Role of a small GTPase Cdc42 in aging and age-related diseases. Biogerontology 2023;24:27–46.
[69] Feng Q, Guo J, Hou A, Guo Z, Zhang Y, Guo Y, et al. The clinical role of serum cell division control 42 in coronary heart disease. Scand J Clin Lab Investig 2023;83:45–50.
[70] Sabe H. KRAS, MYC, and ARF6: inseparable relationships cooperatively promote cancer malignancy and immune evasion. Cell Commun Signal 2023;21:1–7.
[71] Song RX-D, Santen RJ. Membrane initiated estrogen signaling in breast cancer. Biol Reprod 2006;75:9–16.